SCIENCE CHINA
Earth Sciences

• RESEARCH PAPER •

January 2016 Vol.59 No.1: 129–144
doi: 10.1007/s11430-015-5121-7

The causal sequence investigation of the ring current ion-flux increasing and the magnetotail ion injection during a major storm

LU Li[1*], S MCKENNA-LAWLOR[2], CAO JinBin[3], K KUDELA[4] & J BALAZ[2,4]

[1] *National Space Science Center of the Chinese Academy of Sciences, Beijing 100190, China;*
[2] *Space Technology Ireland, National University of Ireland, Maynooth, Co. Kildare, Ireland;*
[3] *School of Astronautics, Beijing University of Aeronautics and Astronautics, Beijing 100191, China;*
[4] *Institute of Experimental Physics, Kosice, Slovakia*

Received December 22, 2014; accepted March 24, 2015; published online June 29, 2015

Abstract Comprehensive records are available in ENA data of ring current activity recorded by the NUADU instrument aboard TC-2 on 15 May, 2005 during a major magnetic storm (which incorporated a series of substorms). Ion fluxes at 4-min temporal resolution derived from ENA data in the energy ranges 50–81 and 81–158 keV are compared with *in situ* particle fluxes measured by the LANL-SOPA instruments aboard LANL-01, LANL-02, LANL-97, and LANL-84 (a series of geostationary satellites that encircle the equatorial plane at ~6.6 R_E). Also, magnetic fields measured simultaneously by the magetometers aboard GOES-10 and GOES-12 (which are also geostationary satellites) are compared with the particle data. It is demonstrated that ion fluxes in the ring current were enhanced during geomagnetic field tailward stretching in the growth phases of substorms rather than after Earthward directed dipolarization events. This observation, which challenges the existing concept that ring current particles are injected Earthward from the magnetotail following dipolarization events, requires further investigation using a large number of magnetic storm events.

Keywords Energetic neutral atoms, Ring current, Energetic particles, Energetic ions injection

Citation: Lu L, McKenna-Lawlor S, Cao J B, Kudela K, Balaz J. 2016. The causal sequence investigation of the ring current ion-flux increasing and the magnetotail ion injection during a major storm. Sci China Earth Sci, 59: 129−144, doi: 10.1007/s11430-015-5121-7

1. Introduction

A typical magnetic storm constitutes a response of the magnetosphere to the arrival at Earth, when the interplanetary magnetic field (IMF) is directed southward, of significantly enhanced solar wind. A storm is initiated when energy transferred into the magnetosphere by the solar wind leads to an intensification of the ring current (Tsurutani and Gonzalez, 1997). The ring current consists mainly of energetic ions and electrons that drift azimuthally in the magnetic field gradient in the inner magnetosphere at radial distances of about 2–7 Earth radii (R_E). The main enhancement in the storm-time ring current occurs at distances of L ~4 (C:son Brandt et al., 2002a; Lu et al., 2008) and is measured using the Dst (or SYM-H) index.

Previous studies have indicated that most ring current ions (including those originating in the solar wind and in the ionosphere), undergo acceleration in the magnetotail, from whence they are injected into the inner magnetosphere (Sergeev et al., 1998; Kamide et al., 1998; Liu and Rostoker, 1995; Daglis et al., 1999). It is noted that only a small number of solar wind ions enter the ring current region directly from the polar cusp (Peroomian and Ashour-Abdalla,

*Corresponding author (email: luli@nssc.ac.cn)

© Science China Press and Springer-Verlag Berlin Heidelberg 2015

1996). Ring current particles are, in this scenario, injected Earthward from the magnetotail by the convection electric field driven by the southward IMF (Wygant et al., 1998, Hori et al., 2005, Xie et al., 2006), and/or the induced electric field associated with sub-storm dipolarization of the geomagnetic field (Delcourt, 2002).

Dipolarization induced electric fields inject particles from the inner plasma sheet to near synchronous altitudes (L>4). The most energetic ions injected from the inner plasma sheet by the convection electric field are transported along open drift paths from the magnetotail to the magnetopause (Xie et al., 2006), where they only form a partial ring current (Le et al., 2004). The source and the paths followed by these ring current ions have posed a puzzle for a long time.

ENA images capable of monitoring spatial variations in the ring current during its temporal evolution, combined with contemporaneous particle measurements made in situ at geostationary orbit, can help in tracing the energetic particle flows that take place during the substorms that characterize major storms. In this regard, C:son Brandt et al. (2002a, 2002b) investigated ion injections into the ring current during serial substorms within a major storm using HENA/IMAGE measurements. These authors using the ENA fluxes observed at L>8 (C:son Brandt et al., 2002a) and inverted ion fluxes at L>9 (C:son Brandt et al., 2002b) in the night side, to explain the particle injections and "substorm growth phase dropouts" they observed near geostationary orbit. But in those works, we noted that the ENA flux observed near the Earth began increasing during the growth phase (C:son Brandt et al., 2002b) and at least before injections (C:son Brandt et al., 2002a).

In the present study the availability of ENA images with high temporal resolution taken by the NUADU instrument aboard the TC-2 spacecraft (McKenna-Lawlor et al., 2004; Liu et al., 2005), complemented by corresponding global ring current ion-flux inversions, has enabled us to follow in detail the process of ring current particle enhancement and decay during a major magnetic storm on 15 May, 2005.

2. The magnetic storm of 15 May, 2005 and contemporaneous NUADU ENA data

Figure 1 shows that on 15 May, 2005, southward directed IMF with accompanying strong solar wind flow pressure drove a major storm, which was marked by a sudden commencement (~0600 UT). This event was accompanied, near its commencement, by two series of sub-storms (at 0608 and 0822 UT), both with amplitude AE ~1800 nT (Tverskaya et al., 2007). According to the AE index (Figure 1), there was another substorm onset at 0736 UT with amplitude AE ~1400 nT. The main phase of the storm was concluded at ~0820 UT when SYM-H=–305 nT. This phase succeeded, but was close to, the onset time of, the last

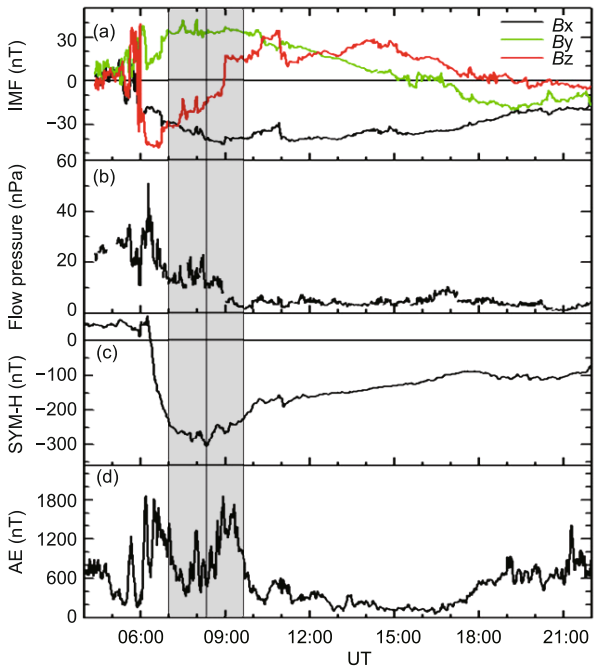

Figure 1 Time variations in the IMF (a), in the flow pressure of the solar wind (b), in the associated SYM-H index (c) and in the AE index (d) on 15 May, 2005. The interval 0700–0944 UT (shaded in gray) defines the period when ENA images were recorded by NUADU/TC2. Three vertical lines separate this interval into two parts. The centre vertical line marks the onset of a substorm at 0822 UT.

substorm mentioned above.

The major storm event considered belongs to the category0020of superstorms. The magnetometer records obtained simultaneously in the auroral and subauroral zones at the time of SC onset substantially differed from activations typically recorded at the beginning of auroral substorms. The extremely large storm on 15 May, 2005 displayed a complex temporal history (e.g., Lazutin and Kuznetsov, 2008 and references therein) and had important consequences in terms of its space weather effects. Initially individual shocks were generated by a pair of successive solar flares. An SC, which occurred at 0230 UT, was followed by an interval characterized by solar wind of variable structure. A second shock, which arrived at Earth at ~0600 UT, initiated a strong "substorm" disturbance. At 0615 UT, IMF B_z changed to negative values. This superstorm is discussed in several papers (e.g., Kozyreva and Kleimenova, 2007). The conditions leading up to such super-intense geomagnetic storms were studied in detail by Echer et al. (2008).

ENA image measurements recorded by the NUADU instrument enable remote monitoring of the evolution of the global ring current. Previous HENA/IMAGE ENA measurement inversions made using long integration times (>10 min) (C:son Brandt et al., 2002b; Lu et al., 2010) masked the causal sequence between ion injection and enhancement of the ring current ion-flux. It is thus of interest to study the behavior of energetic neutral atom images recorded by the

NUADU instrument during this event using shorter integration times which provide both wide angle snapshots and high temporal resolution distributions of energetic ions.

Typical ENA images recorded by NUADU, each of which covers a full 4π solid angle, were recorded in energy channels 50–81 keV and 61–158 keV with spatial resolution 11.5°×2.5° for ~2.7 h (0700–0944 UT) outside the radiation belts near the apogee of TC-2. This observation interval is shaded in gray in Figure 1. The ENA data are routinely cleaned before analysis to remove background noise (McKenna-Lawlor et al., 2010) and thereafter integrated (here over 4 min). In total, 40 integrated ENA images, recorded in two sub-intervals, (a) and (b), for those substorms with commencements at 0736 and 0822 UT respectively, were available in each energy channel and these images are presented in Figures 2 and 3. The ENA fluxes recorded displayed peak values, at 0745 and 0847 UT. The ENA data sampling interval, shaded in gray in Figure 1, is separated into two equal sub-intervals by three vertical lines in Figure 1. The middle vertical line crosses the negative peak of the SYM-H index (Panel 3). This indicates that the sub-interval to the left (sub-interval I, 0700–0822 UT) occurred during the main phase of the "storm" whereas the sub-interval to the right (sub-interval II, 0822–0944 UT) took place during the recovery phase.

3. Ion flux distributions retrieved from NUADU measurements

Constrained linear inversion of the images was achieved using a method designed for NUADU data and described in Lu et al. (2010), with the difference that the present inversions were made using a substantially shorter integration time (4-min) than that previously adopted. Each ENA image (Figures 2 and 3) showed, following the processes of data cleaning and integration, hundreds of ENA counts in the sensitive area around the projected outline of the Earth, thereby satisfying the statistical requirements of the inversion process.

Sequences of ion distributions derived using the constrained linear inversion method at four minute intervals for both sub-interval I and sub-interval II on 15 May, 2005 in the energy ranges 50–81 and 81–158 keV, are presented in Figures 4 and 5, respectively.

Plots in the energy range 50–81 keV (Figure 4(a) and (b)) show ongoing changes in the global ion flux distributions. See in particular, an intense area in the ion fluxes that initially appeared near midnight, then developed to westward, and finally decayed at dusk. The plots in the energy range 81–158 keV (Figure 5(a) and (b)) show two episodes of ion flux evolution in which, in each case, the intensity increased initially on the dusk side (at 0720 and 0822 UT respectively). Thereafter these bright regions each extended eastward, attaining in both cases a maximum on the night side. They then each turned westward and finally decayed on the dusk side. During these changes the most intense areas of the ion fluxes showed internal variations that occurred mainly in the dusk-night sector where two peaks in emission were detected. The first peak occurred at 0745 UT and the second at 0847 UT in the data of both energy channels.

4. Discussion

4.1 Comparison with proton fluxes recorded by LANL/SOPA

The proton fluxes retrieved from NUADU data are shown in Figure 6 superimposed on contemporaneous *in situ* proton flux measurements made aboard the LANL satellites. Purple dots indicate the retrieved proton fluxes in the energy range 50–81 keV and orange dots the retrieved proton fluxes in the energy range 81–158 keV. The proton fluxes deduced from the ENA images are generally consistent with the *in situ* proton measurements made by the LANL-SOPA (Synchronous Orbit Particle Analyzer) instruments. The latter were flown aboard a series of satellites launched by the Los Alamos National Laboratory LANL (Belian et al., 1992) to encircle the equatorial plane at ~6.6 R_E in the environment of the outer radiation belt. Comparisons made with NUADU data using the closest energy range to the *in situ* measurements (marked on the right of each panel of Figure 6) indicate that the retrieved flux values are generally consistent with the *in situ* measurements made by LANL-SOPA: at night (Figure 6(a)), at dusk (Figure 6(b)), and at dawn (Figure 6(d)). The magnetopause was compressed to less than 6.6 R_E at noon during the storm. The dipolar magnetic field model employed in deriving the inversion result (Lu et al., 2010) cannot be employed in the case of the noon measurements (Figure 6(c)) due to the presence at that time of the highly compressed magnetic field configuration.

It is known that, during a storm the magnetic field lines (including the L values) can be stretched tailward (Lu et al., 2010). The further the distance from the Earth, the greater is the deformation produced due to stretching. Thus, the retrieved ion fluxes presented in Figure 6 might be somewhat underestimated. An accurate estimate of the errors cannot be determined. However, the total magnetic field did not change significantly below ~4 R_E (McKenna-Lawlor et al., 2010) and the comparisons in Figure 6, which show that the inverted ion fluxes, were less than, but close to, the *in situ* measurements at geostationary orbit (L ~6.6), providing confidence in the qualitative results of the inversions made around L ~4.

The 4-min temporal resolution adopted enabled us to meaningfully compare the evolution of the ring current ion fluxes with variations in the *in situ* particle measurements. By comparing the *in situ* measurements of LANL-SOPA with the inversion results, we found that proton injections

(a)

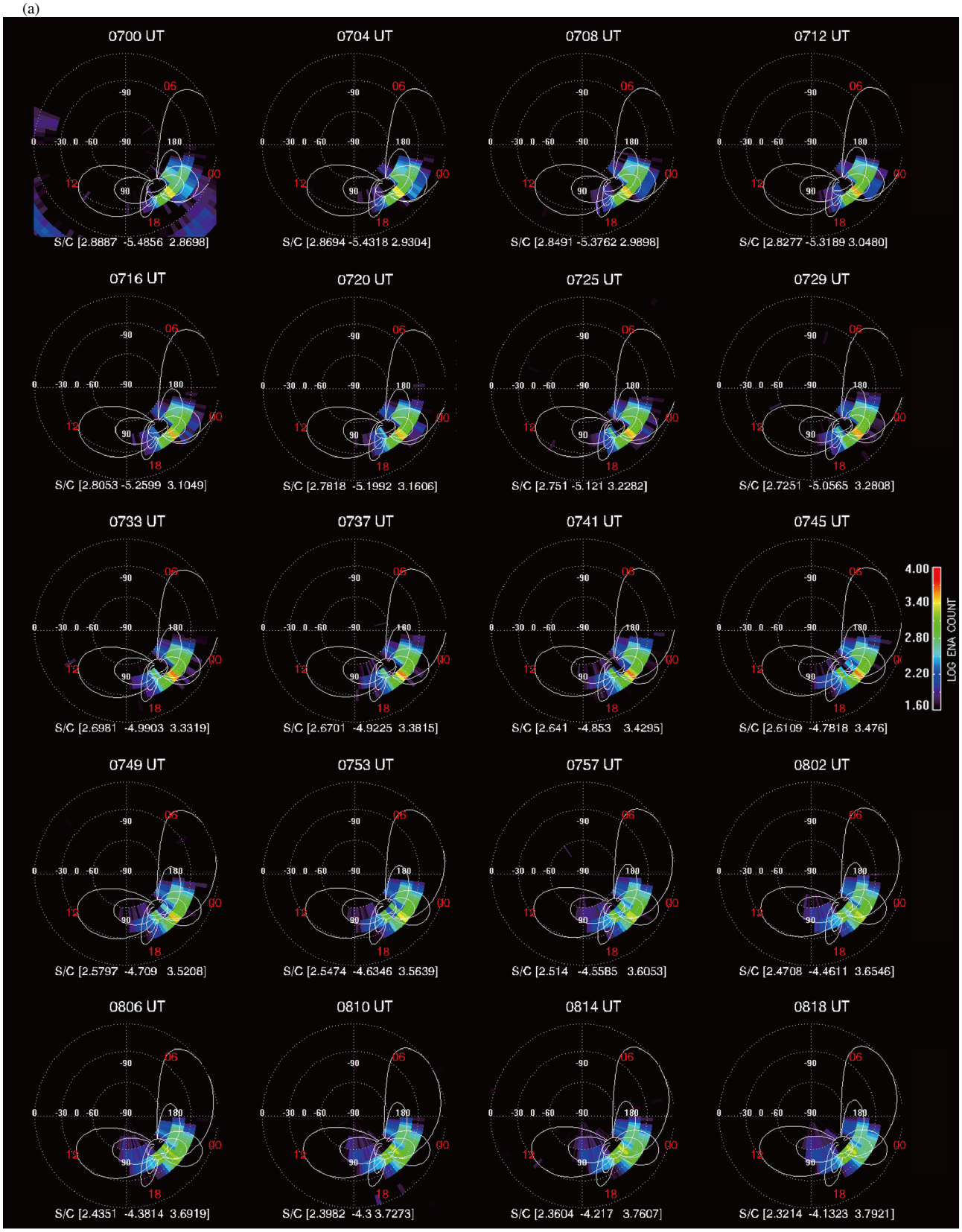

(*To be continued on the next page*)

(*Continued*)

(b)

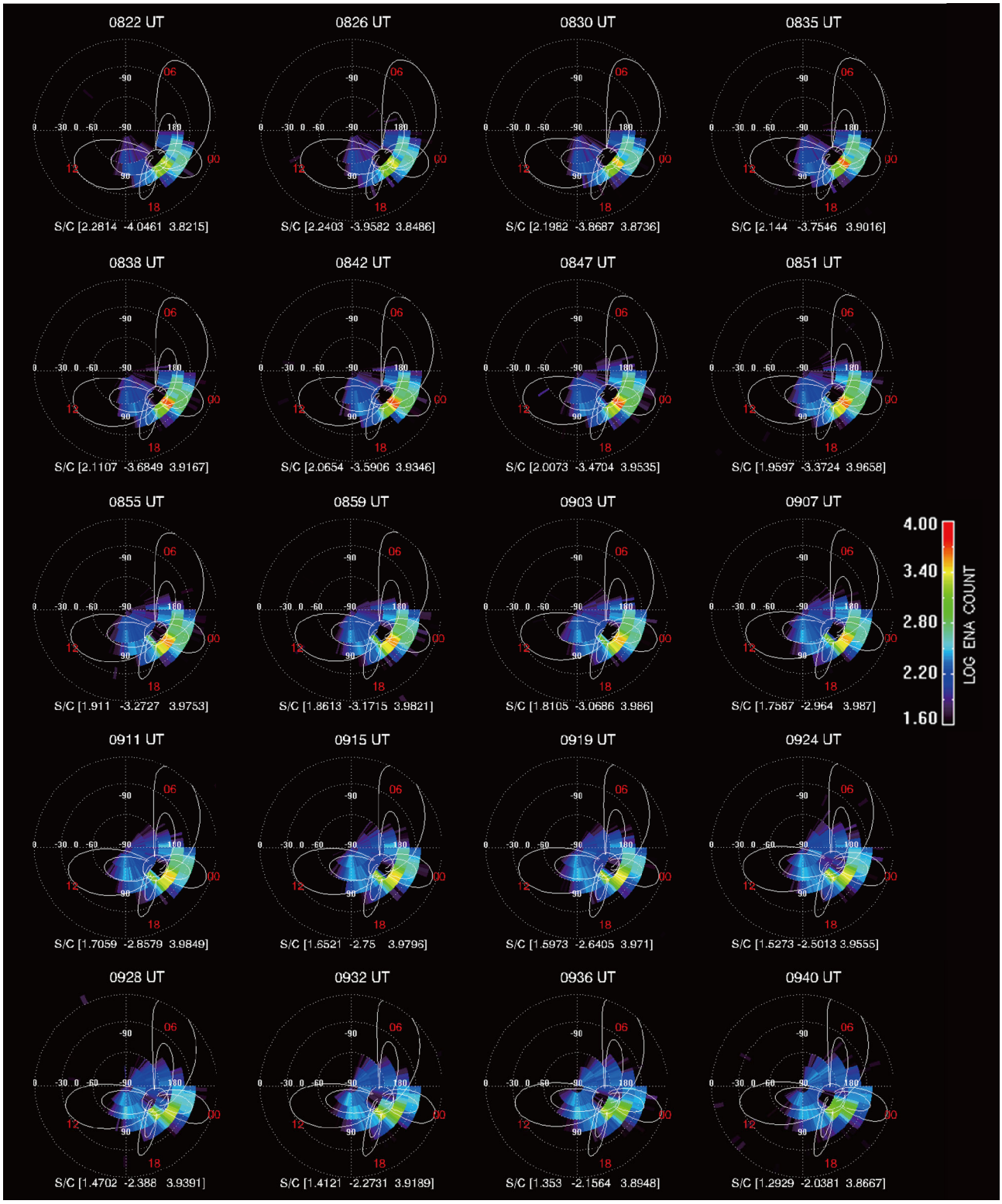

Figure 2 Sequence of ENA images (4-min integration times) recorded by NUADU/TC-2 on 15 May, 2005 in energy channel 50–81 keV during sub-interval I (0700–0822 UT, (a)) and during sub-interval II (0822–0944 UT, (b)). In each panel, the elevation scale is indicated by closed dashed white rings and the azimuth scale by (labeled) dashed lines. Solid white curves represent constant L values (L=4, 8). Four local times are shown in red. The color scale on the right side represents the logarithm of particle counts. The epochs are provided at the top and the positions of TC-2 at the bottom of each panel.

(a)

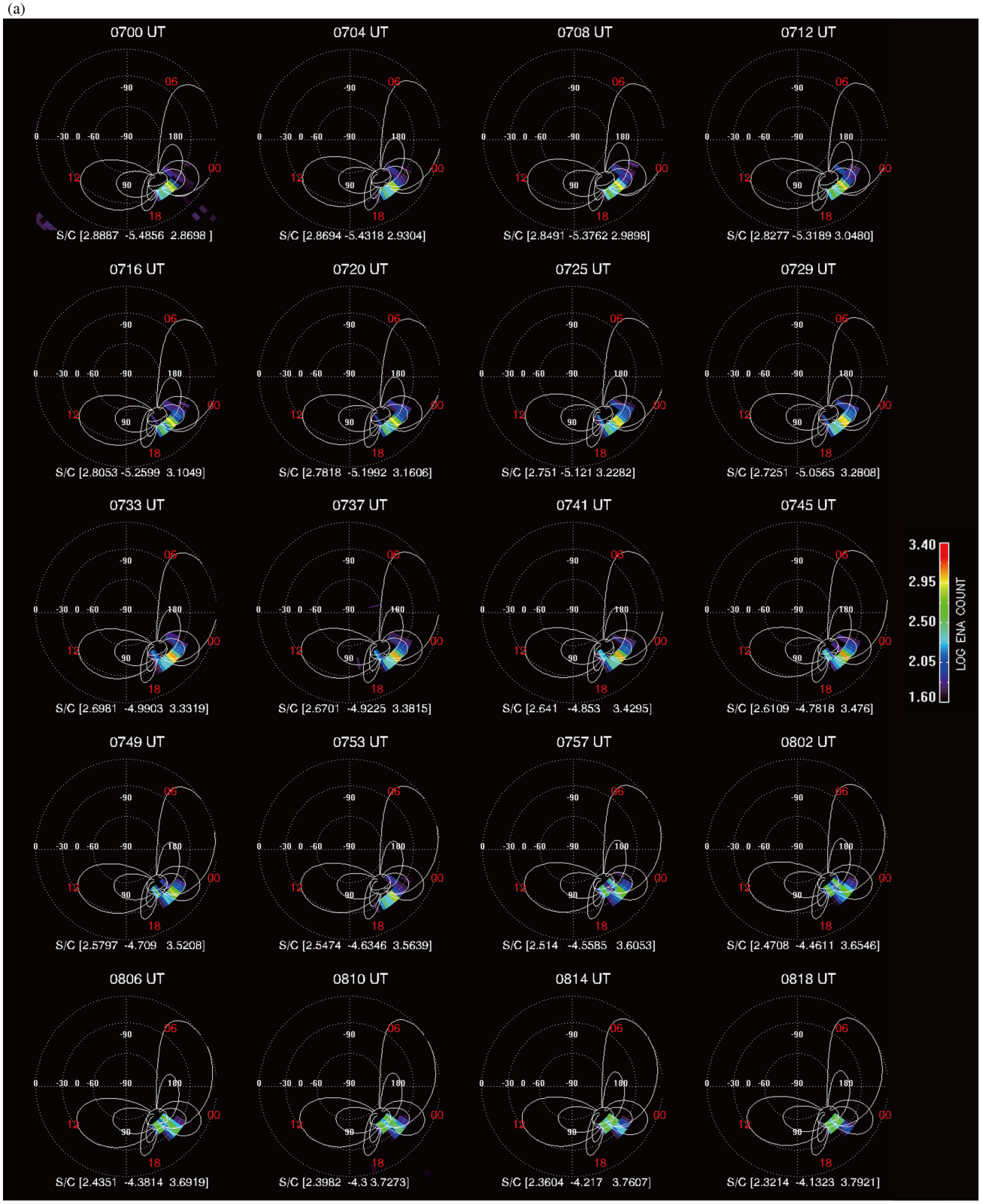

(*To be continued on the next page*)

(*Continued*)

(b)

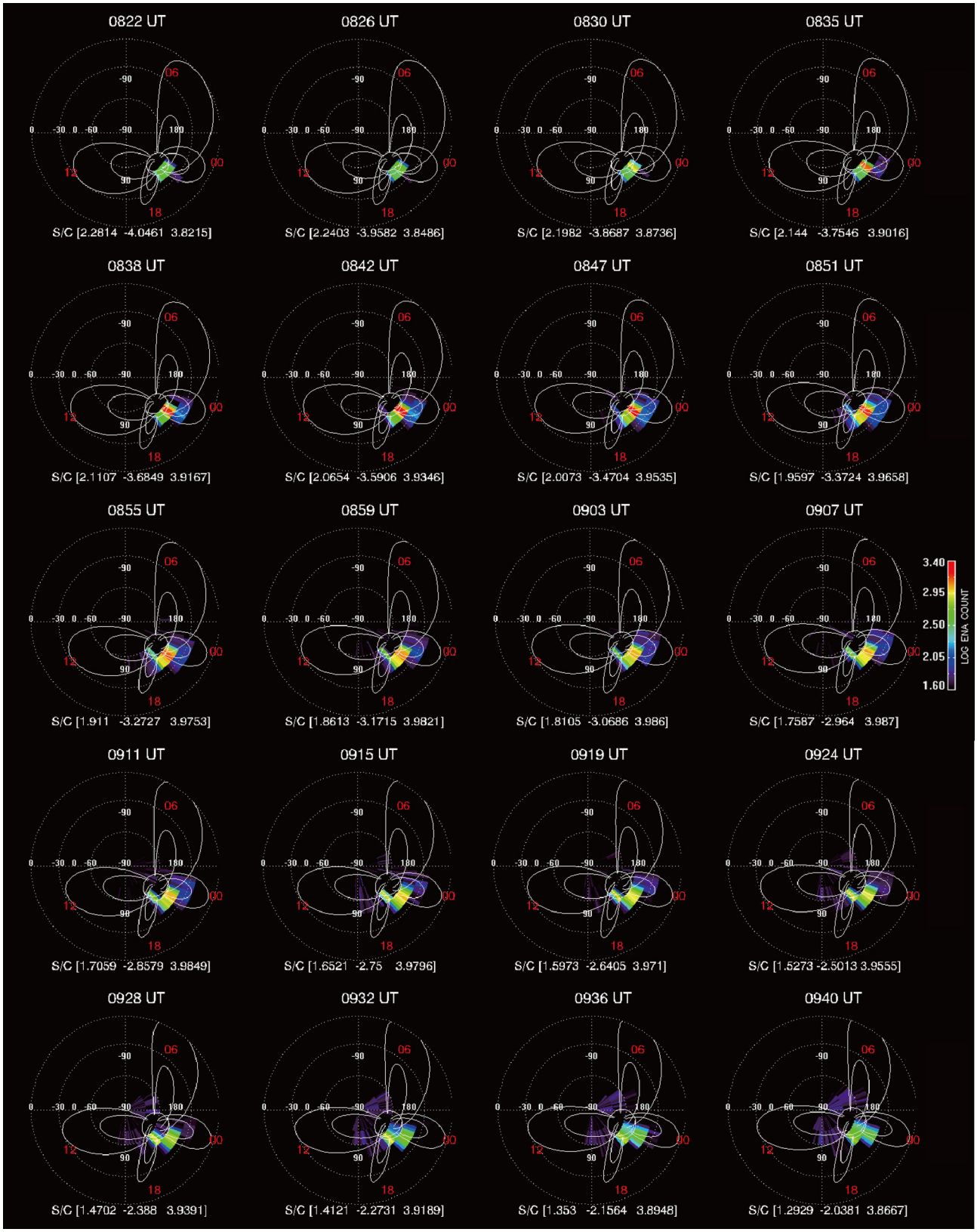

Figure 3 Sequence of NUADU ENA images (4-min integration times) obtained during sub-interval I (0700–0822 UT, (a)) and sub-interval II (0822–0944 UT, (b)) on 15 May, 2005 in energy channel 81–158 keV (displayed using the same format employed in Figure 2).

(a)

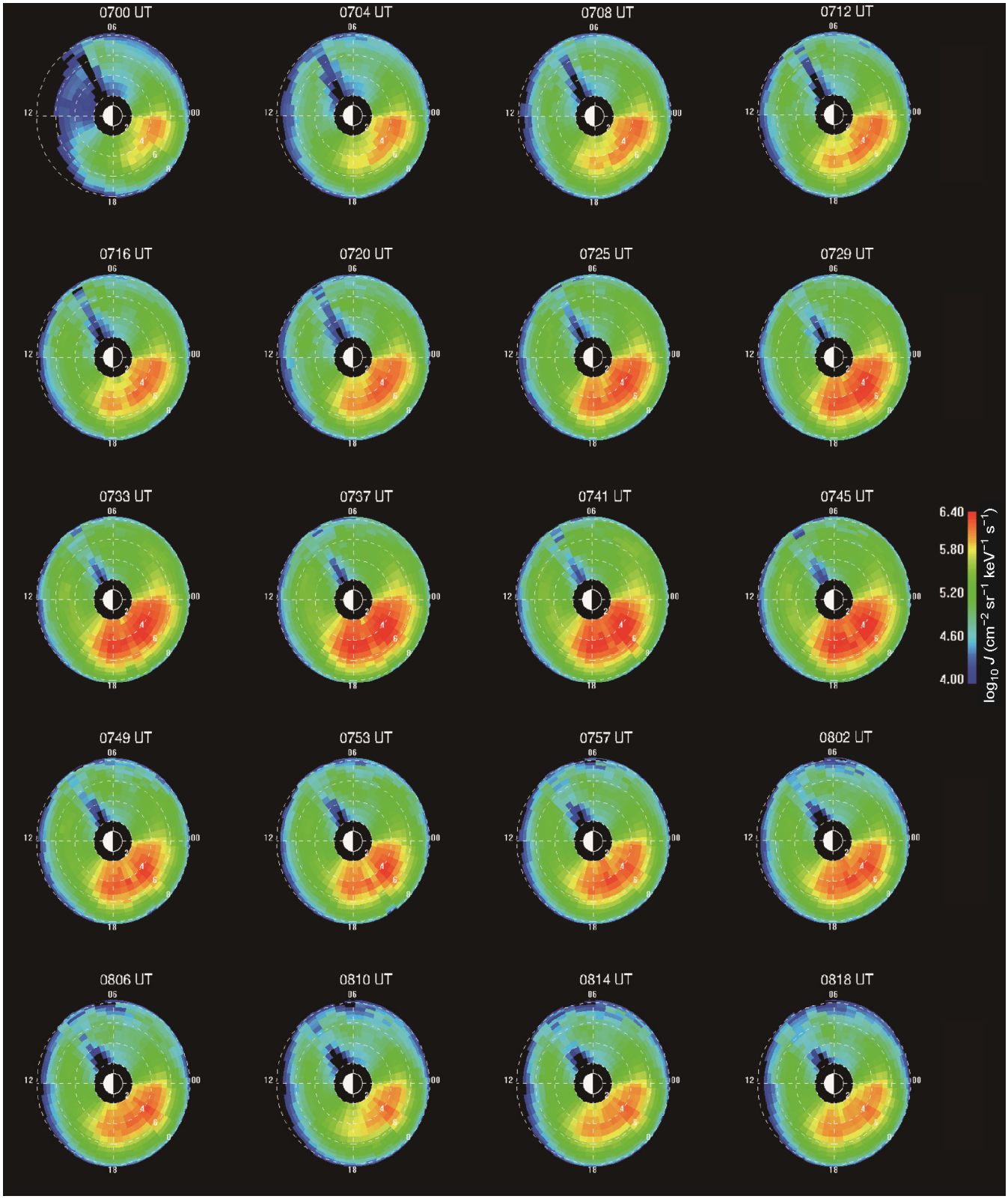

(*To be continued on the next page*)

(*Continued*)

(b)

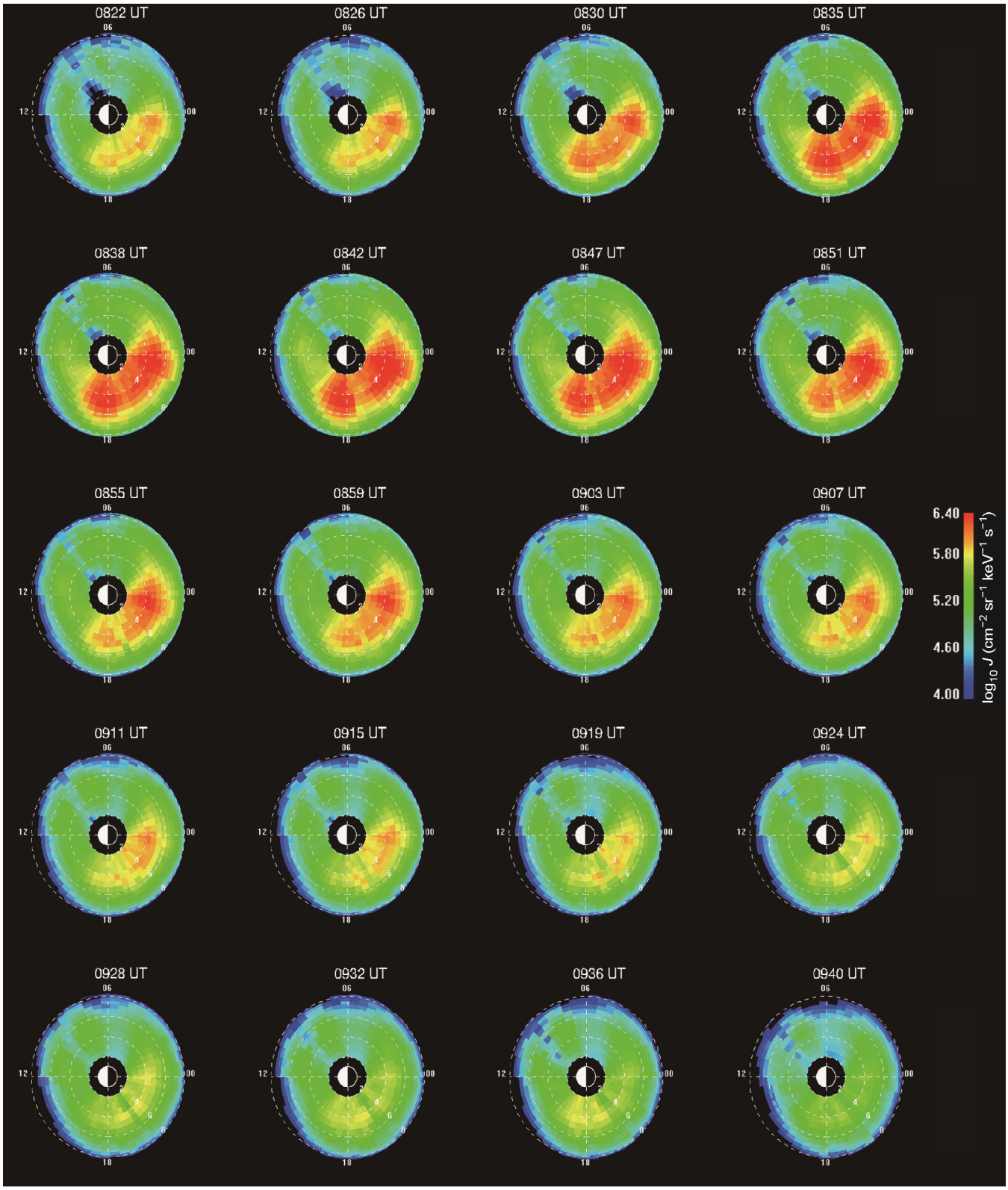

Figure 4 Sequence of retrieved equatorial ion flux (J) distributions (energy range 50–81 keV) obtained for subinterval I (0700–0822 UT, (a)) and subinterval II (0822–0944 UT, (b)) on 15 May, 2005 shown in the L-MLT system. A color scale is provided on the right.

(a)

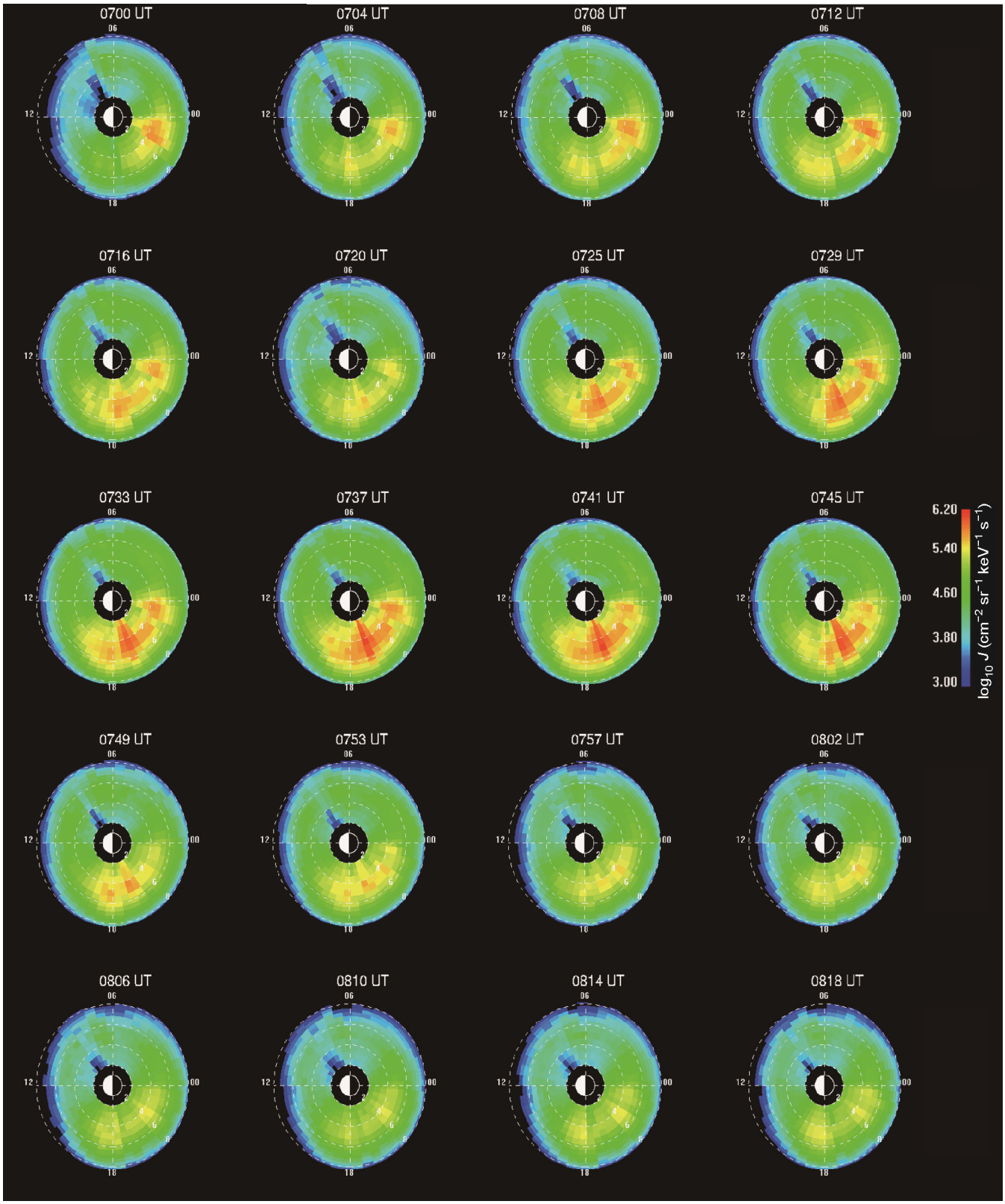

(*To be continued on the next page*)

(*Continued*)

(b)

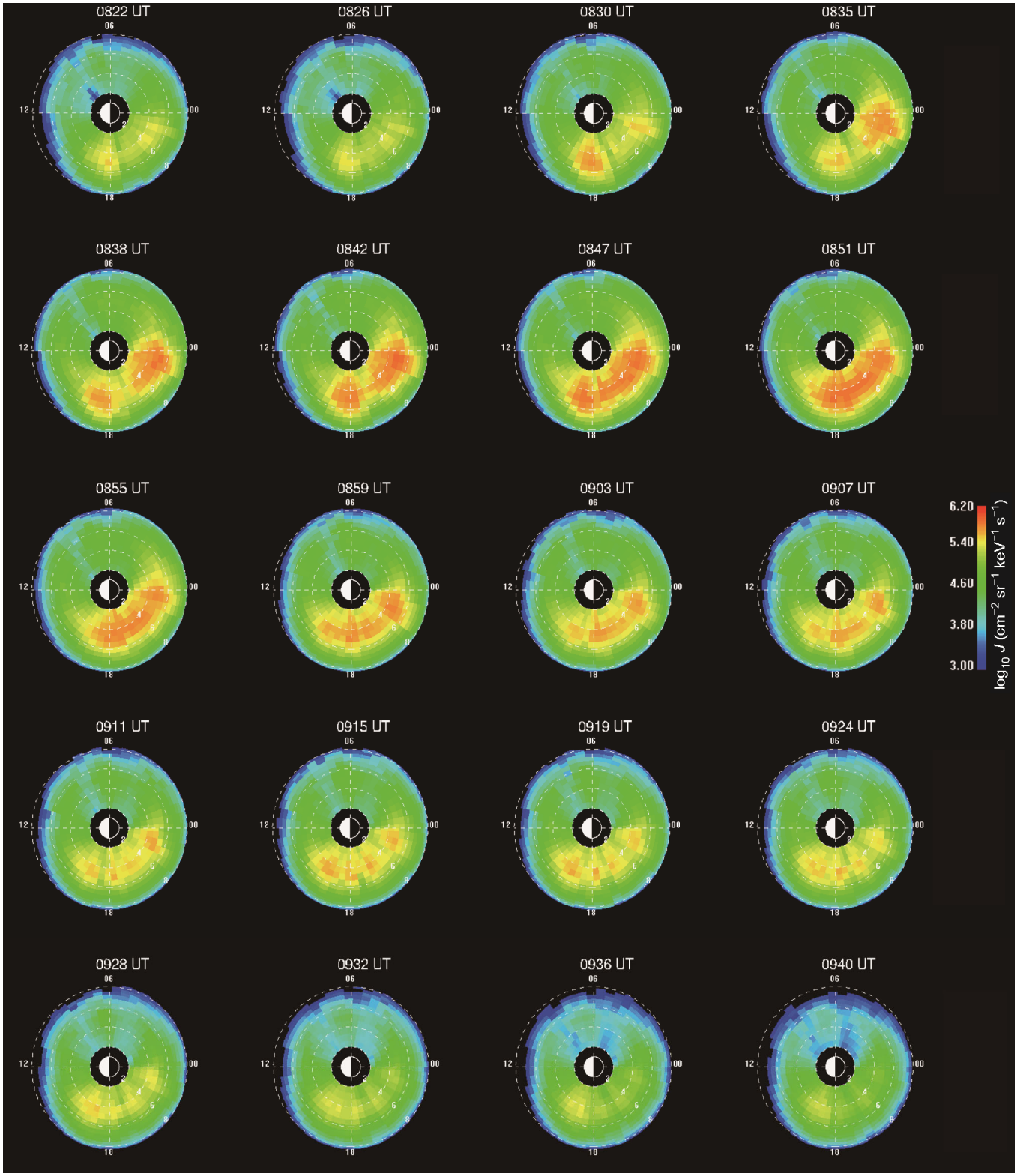

Figure 5 Sequence of retrieved equatorial ion flux (*J*) distributions (energy range 81–158 keV) obtained for subinterval I (0700–0822 UT, (a)) and subinterval II (0822–0944 UT, (b)), displayed in the same format used in Figure 4.

(sharp increases in the proton fluxes measured *in situ*) occurred ahead of ring current ion-flux enhancements at dawn (Figure 6(d)), effectively simultaneously at dusk (Figure 6(b)), and obviously delayed relative to the occurrence of a complementary ring current ion flux increase on the night side (Figure 6(a)). Even by ignoring the time-delay of ENAs from the charge exchange to be recorded remotely, the causal sequence still cannot support the view that ring current ions were injected directly from the inner plasma sheet of the magnetotail.

4.2 Response of the magnetic indices

The ring current is measured in terms of the SYM-H index and it is of interest to see if a correlation is shown with the AU/AL indices that describe series of substorms. The maximum and mean values of the ion fluxes in each panel of Figures 4 and 5 can be used to follow the evolution of the ring current during the storm of 15 May by plotting them in association with several geomagnetic indices (Figure 7). Since the ion flux plots in Figures 4 and 5 have only 4-min temporal resolution, we added as reference material at the bottom of the figure a plot of the maximum ENA counts obtained in the original NUADU measurements. Three vertical black solid lines separate the ENA sampling interval into sub-intervals I and II. Two vertical red dashed lines cross the two peaks in the ion flux curves already mentioned above. Two vertical black dashed lines cross two negative peaks in the AL index in each sub-interval. Two gray shadowed regions cover the time intervals of the ring current ion flux that showed an increase both during the main phase and in the recovery phase of the storm.

Grafe and Feldstein (2000) investigated statistically the relationship between the auroral electrojet intensity (measured

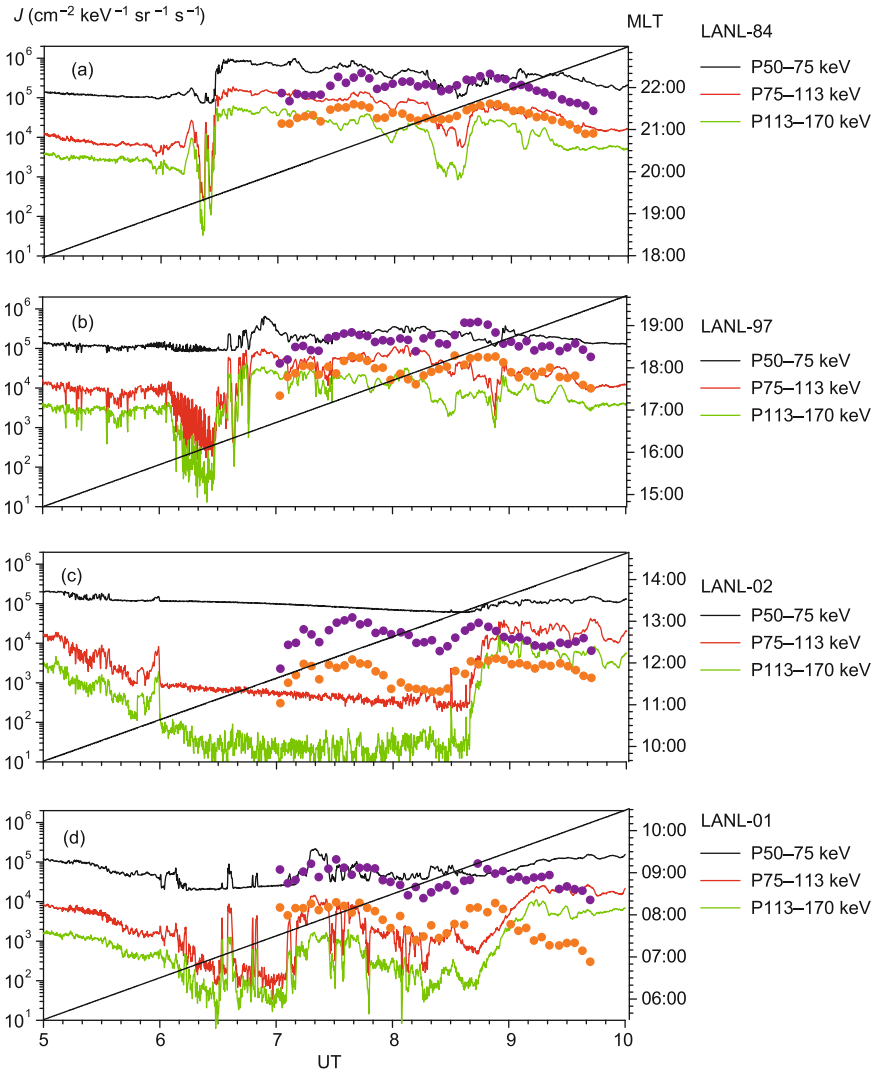

Figure 6 Proton fluxes vs time derived from the ENA images (purple dots in the energy range 50–81 keV and orange dots in the range 81–158 keV) compared with *in situ* measurements made by the LANL-SOPA instruments (the relevant satellite name and the energy ranges of the proton channels concerned are inscribed on each panel). The corresponding magnetic local times are indicated by continuous black lines which are scaled at the right side of the individual panels.

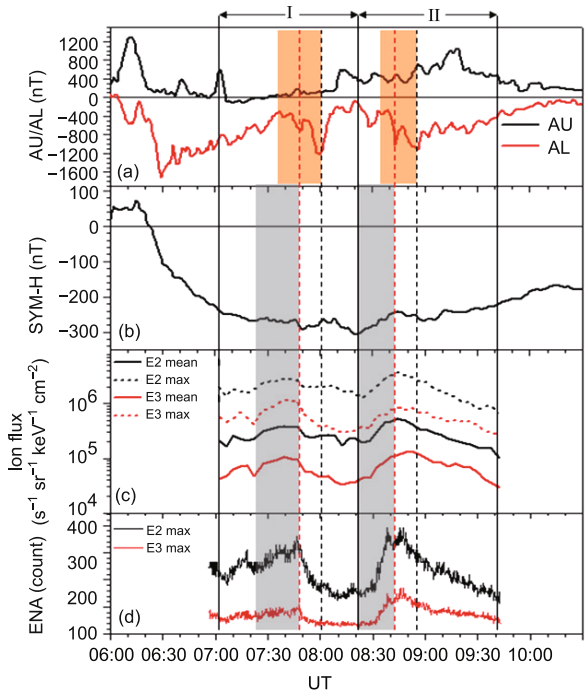

Figure 7 Time variations in the AU/AL indices (a) and SYM-H index (b), the maximum and mean values of equatorial ion fluxes retrieved from ENA measurements (c), and the maximum counts obtained in ENA measurements on 15 May, 2005 (d). Energy channel 50–81 keV is labeled E2 and energy channel 81–158 keV is labeled E3 (for details, see the text).

by the AL-index) and ring current intensity and found no close correlation between these features. In Figure 7, two vertical red dashed lines show that twin peaks in the ion flux curves effectively separate the growth phase from the expansion phase during two consecutive substorms. According to the profile of the AL index, it means that the ion flux enhancement of the ring current was completed in the growth phase of the each substorm. The phases of the AL index (which end with AL bays) are shaded in orange in Figure 7, where they can be seen to have had about the same durations as the ring current ion flux enhancements (shaded in gray in Figure 7), but with an ~12 min delay.

4.3 Ring current evolution in series of substorms

The stretching (blue arrows in Figure 8) and dipolarization (red arrows in Figure 8) of the magnetic field, recorded by magnetometers aboard the GOES-10 (premidnight) and GOES-12 (postmidnight) spacecraft at around midnight, were associated with the growth and expansion phase of a substorm (Liu and Rostoker, 1995; Daglis et al., 1999), which occurred earlier at the geosynchronous altitude as expressed by the AL index (top panel of Figure 7). It seems that the magnetic field response (substorm) had a timing sequence that varied from the magnetotail to the inner magnetosphere. Plasma flows recorded at the geosynchronous altitude refer to LANL-MPA (Magnetospheric Plasma Analyzer) *in situ* measurements (Figure 9).

The magnetic field stretching/dipolarization during substorms were more closely related to a decrease/increase of ion-fluxes at geosynchronous altitudes (Fu et al., 2011, 2012a). Walker et al. (1976) showed that energetic ion flux decreases, at geostationary orbit and around midnight, are usually observed prior to substorm onset. These are followed by particle flux recoveries at substorm onset. These decreases were interpreted as a physical motion of the trapped outer boundary towards a region equatorward and earthwards of the satellite. Sauvaud and Winckler (1980) further showed that this equatorward and earthward motion of the trapped outer boundary is the result of the stretching of the magnetic field lines towards a more tail-like configuration. During each substorm period when magnetic field stretching (blue arrows in Figure 8) and energetic ion-flux

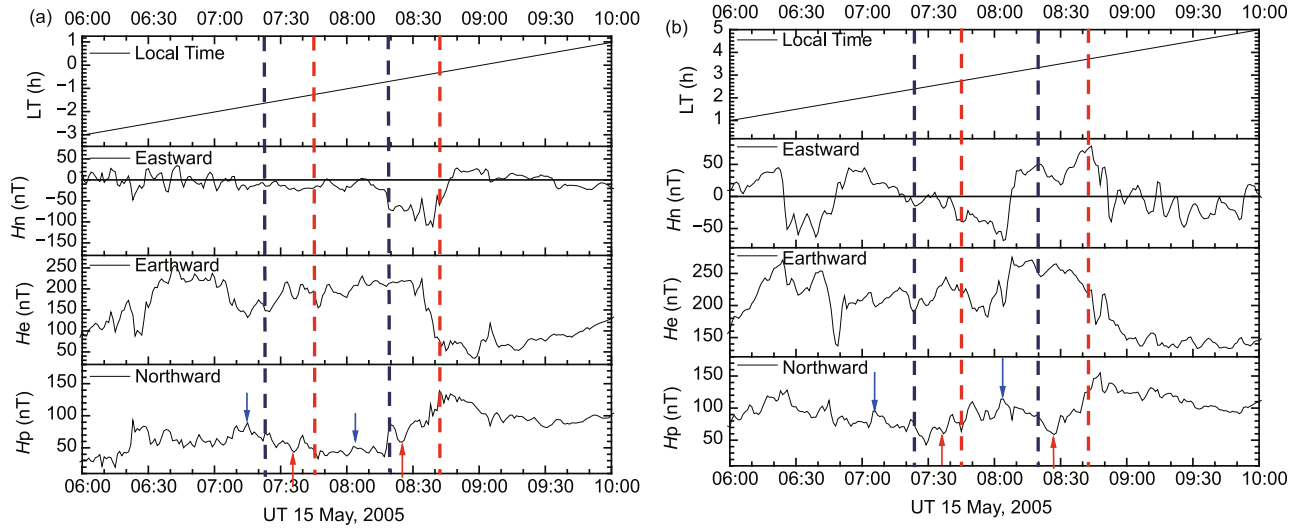

Figure 8 The magnetic field data of GOES-10 (a) and GOES-12 (b) in satellite coordinates, where the top panel in each plot shows the local time. The blue vertical dashed lines show the ring current ion flux increasing points, and the red vertical dashed lines the ring current ion flux peaks.

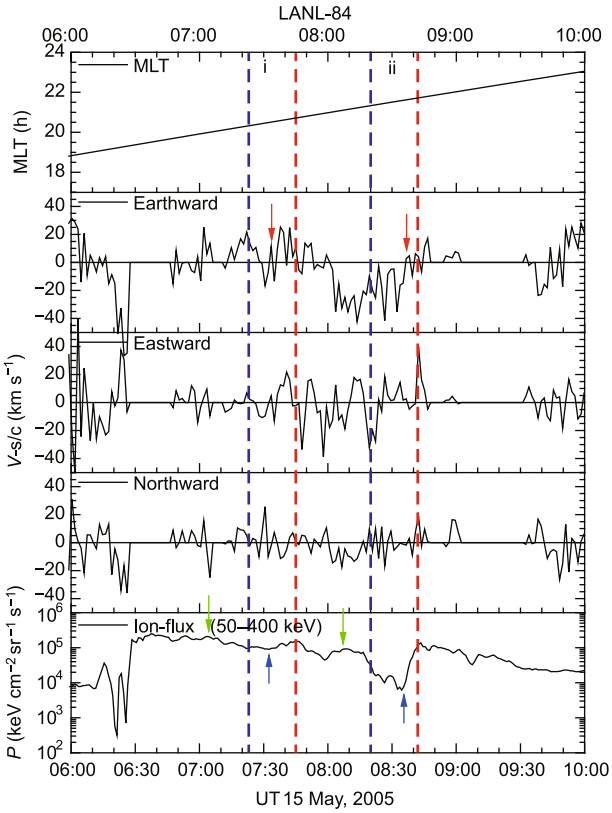

Figure 9 LANL-84/MPA (Magnetospheric Plasma Analyzer) plasma velocity in 3 components (three panels in the middle) in spacecraft coordinates for low energy ions (1–130 eV/e). The top panel show magnetic local time. The bottom panel displays proton flux in the energy range 50–300 keV. The blue and red vertical lines displayed the same as using in Figure 8.

decline at geosynchronous altitudes (green arrows in Figure 9) occurred, this phase constituted a "growth phase dropout" (Sauvaud et al., 1996). Magnetic field dipolarization (red arrows in Figure 8) was accompanied by plasma convective flows turned Earthward (red arrows in Figure 9), and the energetic ion-flux also began to increase rapidly (blue arrows in Figure 9). Such a sharp increase in the energetic ion-flux at geosynchronous altitudes on the night side is understood to represent a ring current ion injection (Sergeev et al., 1998). The time sequences of the various events during the substorms of 0736 and 0822 UT are listed in Tables 1 and 2 respectively. An increase in ring current ion fluxes at a lower altitude (L ~4) occurred earlier (by about 10 min) than the injection signals observed at geosynchronous altitudes. During magnetic field Earthward directed dipolarization events, the convective flows were also directed Earthward.

The ring current with the maximum energetic ion-flux (located at ~4 R_E on the night side) developed during a series of substorms. In the absence of *in situ* magnetic field measurements it is assumed that dipolarization at geosynchronous altitudes propagates inward at the convection speed (Sergeev et al., 1998; Fu et al., 2012b). Figure 10 illustrates schematically that: (1) During stretching, convective flows near geostationary orbit are tailward directed and the magnetic field decreases in the equatorial region. Due to conservation of the first adiabatic invariant, the pitch angles of energetic ions in the magnetotail gradually diffuse adiabatically from "pancake" to "butterfly" as observed at geostationary orbit (Sauvaud and Winckler, 1980), and move Earthward along the field lines to high latitude regions. In the drifting process, some of them are trapped by the inner field lines and bounced into the ring current area. (2) At substorm onset, on dipolarization of the field, particles can retreat back towards geostationary orbit and at the same time high fluxes of freshly injected energetic particles from the tail can come in to intensify the inner magetosphere population.

Injected ions after the dipolarization are trapped, over a broad area by the magnetic field lines in the inner magnetosphere as the trapped outer boundary extending tailward and could not enter the ring current directly. It is seen that for about one hour after the last injection at 0840 UT (bottom panel of Figure 9) the ring current ion fluxes began to decay without any signs of growth observed by the NUADU/TC-2. Only when the solar wind drives the stretching of magnetic field lines tailward can energetic ions

Table 1 Time sequence of various events during the 0736 UT substorm

UT	Spacecraft/instrument	Local time	Descriptions of observational events	Reference
0703	LANL84/SOPA	20:00	Proton fluxes (50–400 keV) start decreasing	Figure 9
0704	Goes12/M-meter	02:06	Magnetic field lines stretch tailward	Figure 8
0714	Goes10/M-meter	22:04	Magnetic field lines stretch tailward	Figure 8
0722	TC-2/NUADU	Global	Ring current ion fluxes begin increasing	Figure 6
0732	LANL84/SOPA	20:31	Proton fluxes(50-400 keV) start increasing	Figure 9
0733	LANL84/MPA	20:33	Convective flows turn Earthward	Figure 9
0735	Goes10/M-meter	22:32	Magnetic field lines show dipolarization	Figure 8
0737	Goes12/M-meter	02:28	Magnetic field lines show dipolarization	Figure 8
0744	TC-2/NUADU	Global	Ring current ion fluxes reach their maximum and start decaying	Figure 6
0800	Ground station		Auroral electrojet, AL-index bay	Figure 7

Table 2 Time sequence of various events during the 0822 UT substorm

UT	Spacecraft /instrument	Local time	Descriptions of observational events	Reference
0803	Goes10/M-meter Goes12/M-meter	23:01 03:03	Magnetic field lines stretch tailward at about the same time	Figure 8
0806	LANL84/SOPA	21:06	Proton fluxes (50–400 keV) start decreasing	Figure 9
0820	TC-2/NUADU	Global	Ring current ion fluxes begin increasing	Figure 6
0825	Goes10/M-meter	23:36	Magnetic field lines show depolarization [a)]	Figure 8
0826	Goes12/M-meter	03:27	Magnetic field lines show dipolarization	Figure 8
0836	LANL-84/MPA	21:36	Convective flows turn earthward	Figure 9
0840	LANL84/SOPA	21:29	Proton fluxes (50–400 keV) show a sharp increase (injection signal)	Figure 9
0842	TC-2/NUADU	Global	Ring current ion fluxes reach their maximum and start decaying	Figure 6
0855	Ground station		Auroral electrojet, AL-index bay	Figure 7

a) Since the growing of *H*p not accompany with *H*n decreasing at 0818 UT, it was not identified as the dipolarization.

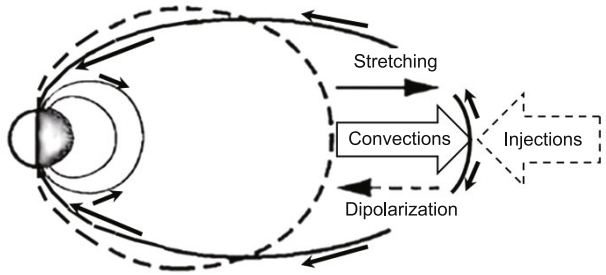

Figure 10 Schematic illustration of the stretching and dipolarization processes during a substorm cycle. Black arrows along the field lines indicate the diffusion of energetic ions during geomagnetic field line stretching.

move Earthward through adiabatic diffusion to reach polar-regions, thereby causing the AE index to increase as the drifting ions finally enter the ring current area.

5 Conclusions

High time resolution ion distributions derived from ENA data recorded by the NUADU instrument aboard TC-2 are available throughout the major magnetic storm of 15 May 2005. Comparisons of these retrieved distributions with in situ measurements of ion-fluxes made aboard spacecraft of the LANL constellation and with magnetic field measurements recorded aboard spacecraft of the GOES constellation (both of which are located in the equatorial plane at ~6.6 R_E in the environment of the outer radiation belt) showed co-variations in the three data sets.

The ring current, measured by Dst index, generated mainly in the high ion flux area near L=4, rather than in the extensive inner magnetosphere area of L<10. High time resolution ion distributions derived from ENA data showed that the evolution of the ring current ion-flux during a major storm was closely related to substorm variations. The magnetic field response of substorms occurred earlier at the geosynchronous altitude on the night side than was the case on the ground. Ring current ion fluxes increased during geomagnetic field stretching in the growth phases of the substorms, rather than after Earthward directed dipolarization events. This observation challenges the current perception that ring current particles are injected directly Earthward from the magnetotail. The "growth phase dropout/injection" signatures observed at geostationary orbit may be interpreted as responses of the trapped outer boundary motion during substorm related stretching/dipolarization events. These conclusions require further investigation using a large number of magnetic storm events.

Acknowledgements *We express many thanks to LANL and GOES missions for use of datum from the internet. This study was supported by the National Natural Science Foundation of China (Grant Nos. 41431071, 41574152), the National Basic Research Program of China (Grant No. 2011CB811404), and the Strategic Priority Research Program on Space Science, the Chinese Academy of Sciences (Grant No. XDA04060201). McKenna-Lawlor S. thanks Enterprise Ireland for also supporting this work. Kudela K. wishes to acknowledge support of grant agency VEGA Project (Grant No. 2/0040/13). Balaz J. thanks agency VEGA Project (Grant No. 2/0059/13) for supporting this work.*

References

Belian R D, Gisler G R, Cayton T E, Christensen R A. 1992. High-Z energetic particles at geostationary orbit during the great solar proton event series of October 1989. J Geophys Res, 97: 16897, doi: 10.1029/92JA01139

C:son Brandt P, Demajistre R, Roelof E C, Ohtani S, Mitchell D G. 2002a. IMAGE/high- energy energetic neutral atom: Global energetic neutral atom imaging of the plasma sheet and ring current during substorms. J Geophys Res, 107: 1454, doi: 10.1029/2002JA009307

C:son Brandt P, Ohtani S, Mitchell D G, Demajistre R, Roelof E C. 2002b. ENA observations of a global substorm growth phase dropout in the nightside magnetosphere. Geophys Res Lett, 29, doi: 10.1029/2002GL015057

Daglis I A, Thorne R M, Baumjohann W, Orsini S. 1999. The terrestrial ring current: Origin, formation, and decay. Rev Geophys, 37: 407–438

Delcourt D C. 2002. Particle acceleration by inductive electric fields in the inner magnetosphere. J Astrophy, 64: 551–559

Echer E, Gonzalez W D, Tsurutani B T. 2008. Interplanetary conditions leading to Superintense geomagnetic storms (Dst≤–250 nT) during solar cycle 23. Geophy Re Let, 35: L06S03, doi: 10.1029/2007GL031755

Fu H S, Khotyaintsev Y V, André M, Vaivads A. 2011. Fermi and betatron acceleration of suprathermal electrons behind dipolarization fronts. Geophys Res Lett, 38: L16104, doi:10.1029/2011GL048528

Fu H S, Khotyaintsev Y V, Vaivads A, André M, Sergeev V, Huang S Y, Kronberg E A, Daly P W. 2012a. Pitch angle distribution of suprathermal electrons behind dipolarization fronts: A statistical overview. J Geophys Res, 117: A12221

Fu H S, Khotyaintsev Y V, Vaivads A, André M, Huang S Y. 2012b. Electric structure of dipolarization front at sub-proton scale. Geophys Res Lett, 39: L06105

Hori T, Lui A T Y, Ohtani S, C:son Brandt P, Mauk B H, McEntire R W, Maezawa K, Mukai T, Kasaba Y, Hayakawa H. 2005. Storm-time convection electric field in the near-Earth plasma sheet. J Geophys Res, 110: A04213

Grafe A, Feldstein Y I. 2000. About the relationship between auroral electrojets and ring current. Ann Geophys, 18: 874–886

Kamide Y, Baumjohann W, Daglis I A, Gonzalez W D, Grande M, Joselyn J A, McPherron R L, Phillips J L, Reeves E G D, Rostoker G, Sharma A S, Singer H J, Tsurutani B T, Vasyliunas V M. 1998. Current understanding of magnetic storms: Storm-substorm relationships. J Geophys Res, 103: 17705–17728

Kozyreva O V, Kleimenova N G. 2007. Geomagnetic pulsations and magnetic disturbances during the initial phase of a strong magnetic storm of May 15, 2005. Geomagn Aeron, 47: 501–511

Lazutin L L, Kuznetsov S N. 2008. Nature of sudden auroral activations at the beginning of magnetic storms. Geomagn Aeron, 48: 165–174

Le G, Russell C T, Takahashi K. 2004. Morphology of the ring current derived from *in-situ* magnetic field measurements. Ann Geophys, 22: 1267–1295

Liu W W, Rostoker G. 1995. Energetic ring current particles generated by recurring substorm cycles. J Geophys Res, 100: 21897–21910

Liu Z X, Escoupet C P, Pu Z Y, Laakso H, Shi J K, Shen C, Hapgood M. 2005. The double star mission. Ann Geophys, 23: 2707–2712

Lu L, McKenna-Lawlor S, Barabash S, Kudela K, Balaz J, Strharsky I, Liu Z X, Shen C, Cao J B, Brandt P C, Tang C L, Dandouras I. 2008. Iterative inversion of global magnetospheric ion distributions using energetic neutral atom (ENA) images recorded by the NUADU/TC2 instrument. Ann Geophy, 26: 1641–1652

Lu L, McKenna-Lawlor S, Barabash S, Brandt P C, Balaz J, Liu Z X. 2010. Comparisons between ion distributions retrieved from ENA images of the ring current and contemporaneous, multipoint ion measurements recorded *in situ* during the major magnetic storm of 15 May 2005. J Geophys Res, 115: A12218

McKenna-Lawlor S, Balaz J, Strharsky I, Barabash S, Brinkfeldt K, Lu L, Shen C, Shi J K, Zong Q G, Kudela K, Fu S Y, Roelof E C, C: son Brandt P, Dandouras I. 2004. The energetic NeUtral Atom Detector Unit (NUADU) for China's Double Star Mission and its calibration. Nucl Instrum Meth A, 530: 311–322

McKenna-Lawlor S, Lu L, Dandouras I, Brandt P C, Zheng Y H, Barabash S, Bucik R, Kudela K, Balaz J, Strharsky I. 2010. Moderate geomagnetic storm (21–22 January 2005) triggered by an outstanding coronal mass ejection viewed via energetic neutral atoms. J Geophys Res, 115, doi: 10. 1029/2009JA014663

Peroomian V, Ashour-Abdalla M. 1996. Population of the near-earth magnetotail from the auroral zone. J Geophys Res, 101: 15387–15401

Sauvaud J A, Winckler J R. 1980. Dynamics of plasma, energetic particles, and fields near synchronous orbit in the nighttime sector during magnetospheric substorms. J Geophys Res, 85: 2043–2056

Sauvaud J A, Beutier T, Delcourt D. 1996. On the origin of flux dropouts near geosynchronous orbit during the growth pahse of substorms: 1. Betatron effects. J Geophys Res, 101: 19911–19920

Sergeev V A, Shukhtina M A, Rasinkangas R, Korth A, Reeves G D,. Singer H J, Thomsen M F, Vagina L I. 1998. Event study of deep energetic particle injections during substorm. J Geophys Res, 103: 9217–9234

Tsurutani B T, Gonzalez W D. 1997. The interplanetary causes of magnetic storms: A review. In: Tsurutani B T, Gonzalez W D, Kamide Y, Arballo J K. Magnetic Storm. Geophysical Monograph Series. Vol. 98. Washington D C: AGU. 77–89

Tverskaya L V, Ginzburg E A, Ivanova T A, Pavlov N N, Svidsky P M. 2007. Peculiarities of the outer radiation belt dynamics during the strong magnetic storm of May 15, 2005. Geomagn Aeron, 47: 696–703

Walker R J, Erickson K N, Swanson R L, Winckler J R. 1976. Substorm-associated particle boundary motion at synchronous orbit. J Geophys Res, 81: 5541–5550

Wygant J, Rowland D, Singer H J, Temerin M, Mozer F, Hudson M K. 1998. Experimental evidence on the role of the large spatial scale electric field in creating the ring current. J Geophys Res, 103: 29527–29544

Xie L, Pu Z Y, Zhou X Z, Fu S Y, Zong Q G, Hong M H. 2006. Energetic ion injection and formation of the storm-time symmetric ring current. Ann Geophys, 24: 3547–3556